Opt Quant Electron (2008) 40:891–905
DOI 10.1007/s11082-009-9290-5

Accurate radial basis function based neural network approach for analysis of photonic crystal fibers

M. F. O. Hameed · S. S. A. Obayya · K. Al-Begain · A. M. Nasr · M. I. Abo el Maaty

Received: 5 September 2008 / Accepted: 12 March 2009 / Published online: 9 April 2009
© Springer Science+Business Media, LLC. 2009

Abstract In this paper, a new and an accurate artificial neural network approach (ANN) is presented for the analysis and design of photonic crystal fibers (PCFs). The new ANN approach is based on the radial basis functions which offer a very quick convergence and high efficiency during the ANN learning. The accuracy of the suggested approach is demonstrated via the excellent agreement between the results obtained using the presented approach and the results of the full vectorial finite difference method (FVFDM). In addition, a new design of highly birefringence PCF with low losses for the two polarized modes is presented using the proposed approach.

Keywords Photonic crystal fibers · Optimization · Artificial neural network · Radial basis function

1 Introduction

Due to their unusual optical properties, photonic crystal fibers (PCFs) (Benabid 2006; Broeng et al. 1999) have attracted the interest of many researchers in recent years. PCFs can be endlessly single mode over a wide wavelength range (Birks et al. 1997), have a large effective mode area (Knight et al. 1998) and can be tailored to achieve nearly zero and flat dispersion over a wide range of wavelengths (Gander et al. 1998). PCFs are usually made of a silica background which contains a regular array of air holes running through the length of the fibre acting as a cladding. This structure creates bandgaps where propagation at certain optical frequencies is forbidden. If the central hole is enlarged (low index core) (Benabid 2006) or removed (high index core) (Broeng et al. 1999), a defect will be produced in the periodic structure. High and low index core PCFs are very promising structures in terms

M. F. O. Hameed · S. Obayya (✉) · K. Al-Begain
Faculty of Advanced Technology, University of Glamorgan, Pontypridd, CF37 1DL, UK
e-mail: sobayya@glam.ac.uk

A. M. Nasr · M. I. Abo el Maaty
Faculty of Engineering, University of Mansoura, Mansoura, Egypt

of properties and possible applications. The low index core PCF can guide the light by the photonic bandgap effect, which allows the confinement of light in its low index core. However this type of PCFs has a narrow wavelength range in which the light is guided and a good accuracy of the periodicity of the lattice is required to obtain a clear bandgap effect. On the other hand, the high index core PCF guides the light by the modified total internal reflection which is much easier to achieve than bandgap guidance. This is due to the fact that the average effective index of the cladding is lower than that of the core.

During the last few years, various accurate modelling methods have been developed for modal analysis of PCFs. These methods included the finite difference time domain (FDTD) (Lizier and Town 2001) which is a powerful technique in dealing with arbitrary-shaped waveguides due to its accuracy and simple implementation. However, it requires large memory and suffers from discretization problems such as staircasing. The finite element method (FEM) (Koshiba and Saitoh 2003; Obayya et al. 2001, 2005) can provide high accuracy by means of flexible triangular and curvilinear meshes to represent the waveguide cross section. However, this accuracy results in an algorithm that is complex to implement. On the contrary the mode solvers based on finite difference method (FDM) (Fallahkhair et al. 2008; Lusse et al. 1994; Yu and Chang 2004) and the multipole method (Campbell et al. 2004; White et al. 2001) are very attractive because of their simple implementations.

The above numerical modal solution techniques are mostly accurate and able to deal with many complex structures including PCFs. However, they are time consuming since they rely on fine meshes for an acceptable accuracy. Saitoh and Koshiba (2005) proposed empirical relations for a simple design of triangular PCFs based on curve fitting technique. In this approach, the normalized frequency V and normalized transverse attenuation constant W were calculated by a vector FEM for PCFs with circular air holes with the same diameter d. Then, empirical relations were invoked to fit the calculated data using the curve fitting. These relations are able to calculate the effective index of the fundamental mode n_{eff}, effective index of the fundamental space-filling mode n_{FSM} and confinement losses of PCFs without using numerical modelling methods. However, these relations are functions only of the wavelength λ and d/Λ ratio (where Λ is the distance between two neighbouring holes) making them useless for elliptical hole PCFs or doped PCFs. In this case, new empirical relations will be required to include the radii of the elliptical holes or refractive index of the doped holes. In addition, the accuracy of the method is restricted to some fitting requirements (Saitoh and Koshiba 2005) such as $\lambda/\Lambda \leq 2, W \geq 0.1$ and $V \geq 0.85$ which limit the applicability of the method. In fact, when the fitting requirements are not satisfied, the empirical relations give values for V and W which deviates from the correct values.

In this paper, a generic analytical approach is proposed for accurately predicting the various mode properties of PCFs such as the effective index, dispersion and confinement losses. The suggested approach depends on using an artificial neural network with radial basis function (ANN-RBF) (Christodoulou and Georgiopoulos 2001). This approach consists of two main steps: training and calculation. In the training stage, the FVFDM is used to calculate the n_{eff} and n_{FSM} for PCF structures with different d/Λ ratios within a certain range of wavelengths. The calculated data will be used in the training process of the ANN-RBF. In the calculation stage, the trained ANN-RBF can be used to calculate the n_{eff} and n_{FSM} of PCF structures for a given d/Λ ratio and wavelength within the trained range without any additional time cost. Consequently, the other modal properties such as the dispersion and confinement losses can be obtained. The use of the radial basis function guarantees a very quick convergence and high efficiency during the ANN training process. In addition, the proposed technique can be used for PCFs with circular, elliptical or doped holes.

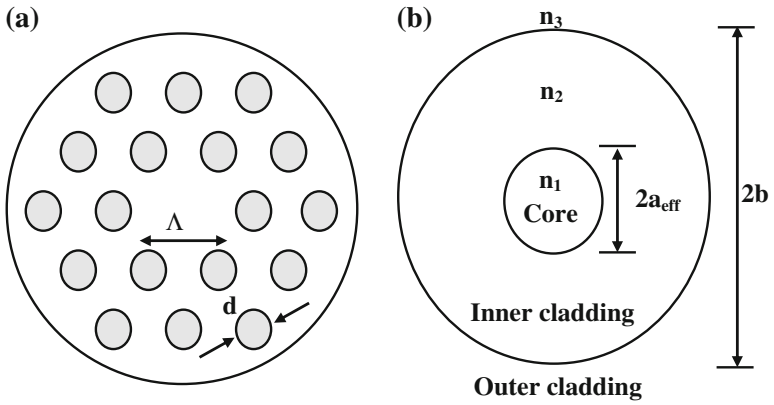

Fig. 1 **a** Cross section of two ring-PCF of 18 air holes (gray area) which are arranged in a silica background (white area). Each hole has a diameter d and the distance between two neighbouring holes is the hole pitch Λ. The corresponding doubly clad fiber is shown in Fig . 1b

In order to prove the efficiency and accuracy of the proposed method, a highly birefringent PCF with low losses for the two polarized modes is proposed and analyzed. The proposed structure offers high birefringence of 0.014 at $\lambda = 1.55\,\mu$m with low losses for the two polarized modes which have been found to be 5.1×10^{-7} and 2.3×10^{-7} dB/m for the TE and TM modes respectively. Moreover, a broad band large normal dispersion which can be used for broad band dispersion compensation is obtained.

The paper is organized as follows. Following this introduction, a brief mathematical treatment of the analytical approach is introduced in Sect. 2. The accuracy and numerical results obtained using the proposed approach will be discussed in detail in Sect. 3. Finally, conclusions are drawn.

2 Analysis

Figure 1 shows the cross section of a PCF with a silica background. The air holes are arranged in a triangular lattice of a hole pitch Λ with the same diameter d. In the proposed approach, the FVFDM (Fallahkhair et al. 2008) is used to obtain the effective index of the fundamental mode n_{eff} and the effective index of the fundamental space-filling mode (FSM) n_{FSM} (Birks et al. 1997; Obayya et al. 2005) for PCF structures with different d/Λ ratios within a certain range of wavelengths. The FSM is defined as the fundamental mode propagating in an infinitely periodic array of air holes in a silica background with no central defect. In this case, only one periodic cell with the appropriate electric and magnetic wall boundary conditions is applied, as shown in Fig. 2. The calculated values of n_{eff} and n_{FSM} are used in the training process of the ANN-RBF. The trained ANN-RBFs can be used to evaluate the n_{eff} and n_{FSM} of PCF structures accurately for a given d/Λ ratio and wavelength within the trained range. Then, V, U and W can be evaluated, as given in the equations below (1)–(3) (Marcuse 1982; Cohen et al. 1982).

$$V = \frac{2\pi}{\lambda} a_{eff} \sqrt{n_{co}^2 - n_{FSM}^2} = \sqrt{U^2 + W^2} \tag{1}$$

$$U = \frac{2\pi}{\lambda} a_{eff} \sqrt{n_{co}^2 - n_{eff}^2} \tag{2}$$

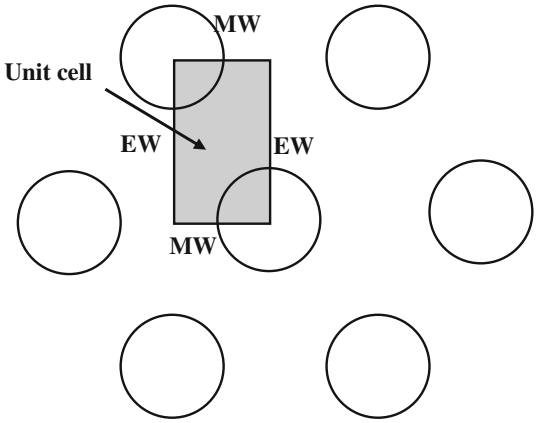

Fig. 2 Schematic diagram of unit cell of the infinitely periodic PCF considered in the FSM mode calculation where EW is a Perfect electric Wall and MW refers to a Perfect magnetic Wall

$$W = \frac{2\pi}{\lambda} a_{eff} \sqrt{n_{eff}^2 - n_{FSM}^2} \tag{3}$$

where, $n_{co} = 1.45$ is the core index value at $\lambda = 1.55\,\mu m$, a_{eff} is the effective core radius which is assumed to be $\Lambda/\sqrt{3}$ (Russell 2003) and the parameter U is the normalized transverse phase constant.

Our aim is to find an accurate method to calculate the n_{eff} and n_{FSM} and hence obtain the other modal properties such as V, U, W, dispersion and confinement losses. It is found that the artificial neural network (ANN) fits for this purpose successfully. The ANN is widely used in many applications (Sood 2004; Christodoulou and Georgiopoulos 2001) such as telecommunications, signal and image processing and control engineering. It consists of input, hidden and output layers. In the suggested approach, the input layer has two neurons in order to define the input parameters λ and d/Λ ratio. The two input parameters and interconnection weights are processed by a summation function and passed first to the transfer function in the hidden layer and then to the output layer. The output layer contains only one neuron in order to define the required parameter, n_{eff} or n_{FSM}. It should be noted that the neural networks must be trained before using them in any calculation. This process is called the learning or training process. Among many types of the learning process, the supervised learning process (Christodoulou and Georgiopoulos 2001) is used in the proposed approach. This process can be described by the following steps:

1. The input parameters are applied at the input layer of the ANN;
2. Initial values for the weights from the hidden to output layers are set to the input parameters;
3. The outputs of the nodes in the hidden and output layers of the ANN are calculated;
4. The mean square error between the calculated outputs of the ANN and the desired outputs is evaluated. If this error is less than a defined error limit, the learning process is terminated. Otherwise, the input weights on each neuron are adjusted by an amount $\Delta\omega_{ij}$ according to the following relation:

$$\Delta\omega_{ij} = \eta[d_j^2(p) - y_j^2(p)]g_i(x(p)) \tag{4}$$

where $d_j(p)$ and $y_j(p)$ are the calculated and desired outputs, respectively, for node j in the output layer, η is the learning rate and $g_i(x(p))$ is the output of the node i at the input layer corresponding to the input x(p).

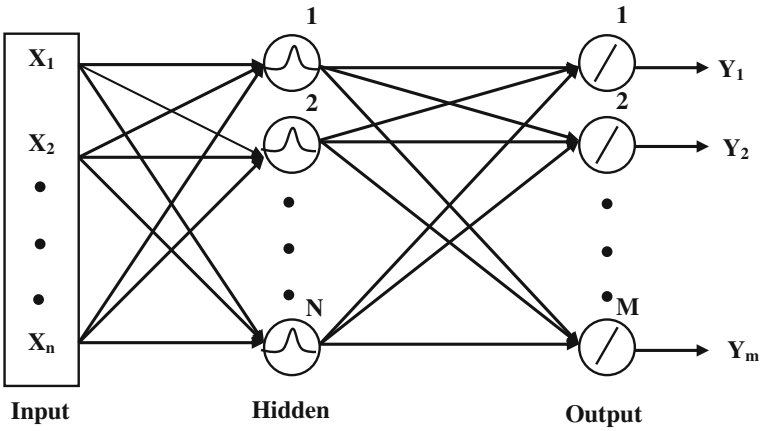

Fig. 3 Schematic diagram of the ANN-RBF

In this paper, two different ANN procedures will be discussed thoroughly, the conventional ANN and ANN-RBF. The conventional ANN contains a linear transfer function in the input and output layers, while the hidden layer consists of a number of neurons with a Log sigmoid transfer function defined as $f(x) = 1/(1 + e^{-x})$. The ANN-RBF used in the suggested approach, as shown in Fig. 3, uses Gaussian transfer function as radial basis function in the hidden layer. The output of the hidden layer of the ANN-RBF is given by Sood (2004) as:

$$O_k = \exp\left(-\frac{[x - c_k]^T[x - c_k]}{2\sigma^2 k}\right) \tag{5}$$

where $k = 1, 2, \ldots, N$ (where N is the number of hidden nodes), O_k is the output of the kth node of the hidden layer, x is the input pattern vector, c_k is the centre of RBF of kth node of hidden layer and σ_k is the spread of the kth RBF. Figure 3 shows also that the output layer of the ANN-RBF contains a linear transfer function. The output of the jth ANN-RBF is

$$Y_j = \omega_j O_j \tag{6}$$

where $j = 1, 2, \ldots, M$ (where M is the number of output nodes), Y_j is the output of jth node, ω_j is the weight vector for node j and O_j is the vector output from the jth hidden layer. On the contrary of conventional ANN which uses a fixed number of neurons in the hidden layer, during the learning process of the ANN-RBF a new neuron is added to the hidden layer until the error condition is fulfilled.

3 Results

The suggested approach with the conventional ANN and ANN-RBF has been applied initially to different PCF structures in order to compare their numerical performances. In order to start the training process, n_{eff} of a PCF with $\Lambda = 2.3\,\mu m$ for d/Λ ratios equal to 0.5, 0.6 and 0.7 are computed using the FVFDM over a range of wavelengths from 0.1 µm to 1.9 µm with step 0.3 µm for each d/Λ ratio. The calculated data are then used for the training process of the conventional ANN. Once the training process is completed, the trained ANN will be

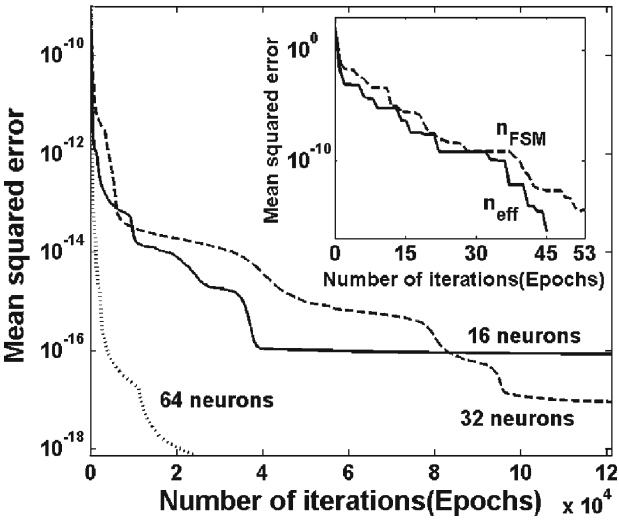

Fig. 4 The variation of the mean square error between the desired output and output of the conventional ANN for the n_{eff} with the number of iterations during the training process with different number of neurons at the hidden layer as a parameter. The inset figure shows the variation using the ANN-RBF for n_{eff} and n_{FSM}

able to calculate the n_{eff} at a given d/Λ ratio within the range from 0.5 to 0.7 at a particular wavelength within the trained range. For this example, the input layer of the conventional ANN consists of a linear transfer function and two input neurons which represent the input parameters λ and d/Λ ratio, respectively. The hidden layer consists of 16 neurons with a Log sigmoid transfer function, while the output layer consists of a linear transfer function and one neuron in order to define the n_{eff}. To test the consistency and accuracy of the trained ANN, the n_{eff} for the trained value $d/\Lambda = 0.6$ and untrained value 0.63, both over the range of wavelengths from 0.1 µm to 1.9 µm, are calculated using the trained ANN and compared with those obtained using the FVFDM. The comparison was performed using the error percentage in n_{eff} defined as $(n_{eff\,FVFDM} - n_{eff\,ANN}) \times 100\%/n_{eff\,FVFDM}$. The computed error percentages for $d/\Lambda = 0.6$ and 0.63 were within $10^{-6}\%$ and 3% respectively. The percentage error values reveal that the trained ANN is consistent which is indicated by the very low error obtained for $d/\Lambda = 0.6$ which means that a correct result is obtained every time a trained data is used as an input. However, the trained ANN has low accuracy at $d/\Lambda = 0.63$ which is pointed out by its large error which means that poor accuracy is obtained every time an untrained data is used as an input. In order to investigate the effect of increasing the number of neurons in the hidden layer on the accuracy of the conventional ANN, two other different ANNs, with 32 and 64 neurons in the hidden layer, were used. The two new ANNs are trained and in Fig. 4 the training curves are shown and compared with the case of 16 neurons. As seen from this figure, the mean square error between the output of the conventional ANN and the desired output during the training process decreases with increasing the number of neurons. Therefore, the performance of the designed ANN is enhanced by increasing the number of the neurons in the hidden layer. The error percentages in n_{eff} for $d/\Lambda = 0.6$ have been found to be 1×10^{-6}, 0.3×10^{-6} and $0.17 \times 10^{-6}\%$ using 16, 32 and 64 neurons respectively. However, the error percentages for $d/\Lambda = 0.63$ were 3, 0.04 and 0.005% using 16, 32 and 64 neurons respectively. It is apparent from the error values that the trained conventional ANN with 64 neurons in the hidden layer offers the highest accuracy for both trained and

untrained data. The learning process using 64 neurons takes about 876.4 s of CPU time using a personal computer (Pentium(R) D CPU 2.8-GHz, 2.79 GHZ, 1 GB of RAM) until the mean square error between the calculated output of ANN-RBF and desired output reaches a fixed error limit. It should be noted that the time taken by the FVFDM is not included. In order to decrease the time taken in the learning process, another ANN technique was required.

The ANN-RBF is widely used in many applications (Sood 2004; Christodoulou and Georgiopoulos 2001) such as telecommunications, signal and image processing, and control engineering. To the best of the authors' knowledge, this is the first time that the ANN-RBF is employed in the analysis of photonic devices. An ANN-RBF was trained using the calculated n_{eff} of a PCF with $\Lambda = 2.3\,\mu m$ for d/Λ ratios equal to 0.5, 0.6 and 0.7 over a range of wavelengths from 0.1 µm to 1.9 µm with step 0.3 µm for each d/Λ ratio. It is found that the learning process takes only about 0.44 s of CPU time with 45 neurons at the hidden layer until the mean square error between the calculated output from the ANN-RBF and the desired output reaches a fixed error limit. This shows clearly that the learning process of the ANN-RBF takes mush shorter time compared to the conventional ANN. The same procedure was carried out for designing ANN-RBF for calculating n_{FSM}. The inset of Fig. 4 shows the training curves of the n_{eff} and n_{FSM} using the ANN-RBF. As shown from this figure, that the learning process needs only 45 and 53 iterations (epochs) for the n_{eff} and n_{FSM} respectively to reach the required error limit which points out the fast learning process of the ANN-RBF. The percentage errors for $d/\Lambda = 0.6$ and 0.63 between the n_{eff}, n_{FSM} and dispersion calculated by the FVFDM and those obtained by the two ANNs; conventional ANN with 64 neurons in the hidden layer and ANN-RBF are presented in Tables 1 and 2. It can be observed from these tables that both ANNs have a comparable accuracy while, the ANN-RBFs have a very quick convergence. In addition, both ANNs offer high accuracy for $d/\Lambda = 0.6$ and 0.63 which ensures that they are consistent and accurate. The trained ANNs can then evaluate n_{eff} and n_{FSM} accurately at a given d/Λ ratio from 0.5 to 0.7 at a particular wavelength from 0.1 µm to 1.9 µm without any extra time. This overcomes the meshing problems and computational time of the other modelling methods. A limit of the suggested approach is that a numerical method is still required to obtain accurate modal properties for PCF structures for the training process.

In order to prove that the suggested approach can deal accurately with more than two dimensional problems, the following example will be introduced. In this case, the input layer has three neurons in order to define the input parameters λ, d/Λ ratio and Λ while the output layer contains only one neuron in order to define the required parameter n_{eff}. In this example,

Table 1 The percentage errors for $d/\Lambda = 0.6$ between the calculated values of n_{eff}, n_{FSM} and dispersion by the FVFDM and those which are obtained by the two ANNs; conventional ANN and ANN-RBF. The included time is the time required for the learning process. In addition, the indicated numbers of neurons are the number of neurons in the hidden layer. The hole pitch of the PCF is kept constant at 2.3 µm

Parameter	Conventional ANN			ANN-RBF		
	Number of neurons	Error (%)	CPU time (s)	Number of neurons	Error (%)	CPU time (s)
n_{eff}	64	$\pm 1.7 \times 10^{-7}$	876.4	45	$\pm 3.0 \times 10^{-8}$	0.44
n_{FSM}	64	$\pm 2.0 \times 10^{-7}$	945.5	53	$\pm 1.5 \times 10^{-7}$	0.64
Dispersion	–	$\pm 2.0 \times 10^{-3}$	–	–	$\pm 1.0 \times 10^{-3}$	–

Table 2 The percentage errors for $d/\Lambda = 0.63$ between the calculated values of n_{eff}, n_{FSM} and dispersion by the FVFDM and those which are obtained by the two ANNs; conventional ANN and ANN-RBF. The hole pitch of the PCF is kept constant at 2.3 µm

Parameter	Error (%)	
	Conventional ANN	ANN-RBF
n_{eff}	± 0.005	± 0.006
n_{FSM}	± 0.03	± 0.034
Dispersion	±1	±1

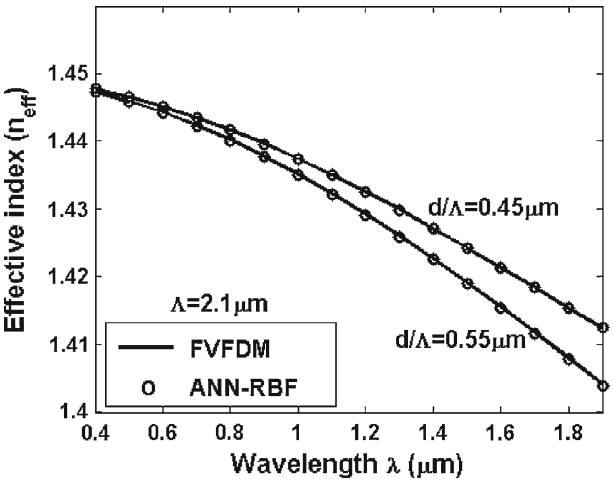

Fig. 5 The variation of the effective index n_{eff} of four-ring PCF with the wavelength at two different d/Λ ratios, 0.45 and 0.55, while Λ is kept constant at 2.1 µm

the suggested approach deals with a three dimensional problem. In order to start the training process, n_{eff} of PCF structures with different hole pitch Λ, 2.0 µm, 2.2 µm and 2.4 µm, are computed using the FVFDM. Each hole pitch is used over a range of wavelengths from 0.1 µm to 1.9 µm with step 0.3 µm for d/Λ ratios equal to 0.4, 0.5 and 0.6. The calculated data are then used for the training process of the ANN-RBF. Once the training process is completed, the trained ANN-RBF will be able to calculate the n_{eff} for PCF structures with a given d/Λ ratio in the range from 0.4 to 0.6 with a selected hole pitch within the range from 2.0 µm to 2.4 µm at a particular wavelength in the range from 0.1 µm to 1.9 µm. Figure 5 illustrates the variation of the n_{eff} with the wavelength at d/Λ ratio equals to 0.45 and 0.55 with Λ fixed to 2.1 µm. It should be noted that the previous values do not represent a trained data. It is evident from this figure that there is a good agreement between the data calculated by the FVFDM and that obtained from the ANN-RBF which proves the accuracy of the trained ANN-RBF.

Next, the proposed approach using the ANN-RBF has been applied for studying the other modal properties of PCFs such as confinement losses, birefringence and dispersion. The confinement loss in dB/m can be obtained using

$$\text{Confinement loss} = 4.342945(2\alpha)\text{dB/m} \tag{7}$$

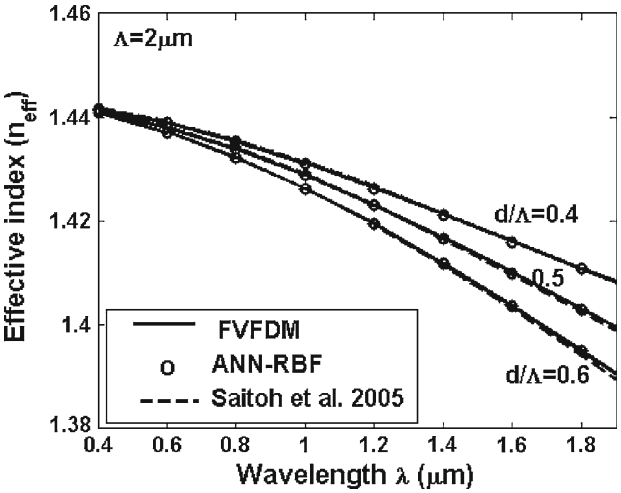

Fig. 6 The variation of the effective index n_{eff} of four-ring PCF with the wavelength at different d/Λ ratios, 0.4, 0.5 and 0.6, while Λ is kept constant at 2.0 μm

where 2α is the power leakage loss which can be calculated using the following relation (Cohen et al. 1982; Marcuse 1982)

$$2\alpha = \frac{2\lambda U^3 W}{n_{eff} a_{eff}^2 V^4 K_1^2(W)} \exp\left(-\frac{2bW}{a_{eff}}\right) \tag{8}$$

where K_1 is the modified Bessel function of the second kind and b is the effective inner-cladding radius. In order to calculate the value of b, the PCF structure is replaced by a doubly clad fiber as shown in Fig. 1.b, where n_1, n_2 and n_3 are the refractive indices of the core, inner cladding, and outer cladding respectively, and a_{eff} is the effective core radius. The outer cladding index is assumed to be the same as the core index $n_1 = n_3 = n_{co} = 1.45$ at $\lambda = 1.55$ μm. In addition, the inner cladding index is expressed by the effective index of the so called fundamental space filling mode, $n_2 = n_{FSM}$. Using this approximation, the value of b can be obtained from

$$S_N = \pi(b^2 - a_{eff}^2) = \left(\frac{\sqrt{3}}{2}\right)\Lambda^2 \sum_{I=1}^{N} 6I \tag{9}$$

where S_N is the area of the inner-cladding and N is the number of hole rings. Figures 6 and 7 illustrate the variation of the n_{eff} and confinement loss of four-ring PCF with the wavelength for different d/Λ ratios, 0.4, 0.5 and 0.6, while Λ is kept constant at 2.0 μm using ANN-RBF, FVFDM and those obtained from the empirical relations (Saitoh and Koshiba 2005). From these figures, it is clear that there is a good agreement between the ANN-RBF results and those obtained from the numerical modal techniques.

The birefringence has also been studied using the proposed approach. The birefringence can be defined as the difference between the effective indices of the two fundamental modes H_{11}^y and H_{11}^x as given below:

$$B = |n_y - n_x| \tag{10}$$

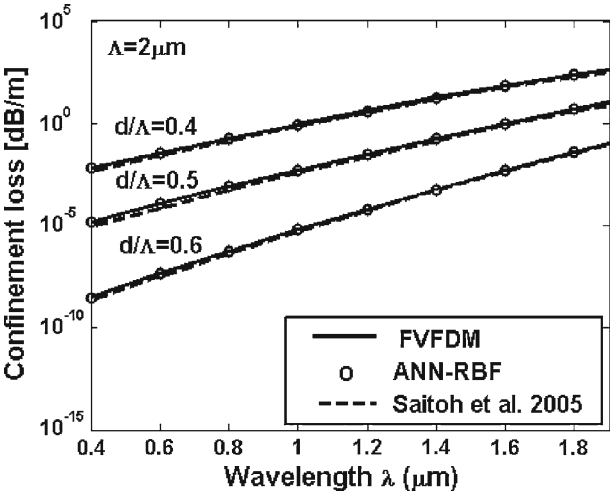

Fig. 7 The variation of the confinement loss of four-ring PCF with the wavelength at different d/Λ ratios, 0.4, 0.5 and 0.6, while Λ is kept constant at 2.0 μm

where n_x and n_y are the effective indices of the two fundamental polarized modes. The birefringence would be enhanced by introducing asymmetry in the structure of the PCF. This can be achieved either by using elliptical holes (Hansen et al. 2001; Yue et al. 2006, 2007) or by the material of the fibre itself (Tsai et al. 1991). PCFs with high birefringence are commonly used in many applications such as optical communication systems and polarization maintaining fibers in sensing applications (Nakazawa 1985). There are many structures which have been reported previously in the literature to achieve high birefringence in PCFs at the operating wavelength $\lambda = 1.55\,\mu m$. Suzuki et al (Suzuki et al. 2001) introduced two bigger holes in the first ring which gave a birefringence of 1.4×10^{-3}. In addition, the use of elliptical holes (Steel and Osgood 2001) results in a birefringence of 2.035×10^{-3}. Furthermore, the elliptical PCF with two bigger holes in the first ring (Yue et al. 2006) produces a birefringence of 5.494×10^{-3}. Moreover, Yang Yue et al. (Yue et al. 2007) reported the birefringence of 3.78×10^{-2} at $\lambda = 1.55\,\mu m$ for a squeezed hexagonal lattice with elliptical holes. Although the above structures exhibit a highly birefringence, there are some limitations in using elliptical holes due to the difficulty of their fabrication.

The cross section of the proposed highly birefringence PCF is shown in Fig. 8. It consists of a squeezed four ring-PCF with $\Lambda_y = 1.7\,\mu m$ and $\Lambda_x = 1.65\,\mu m$ where, Λ_x and Λ_y are the hole pitches in x and y direction respectively. Also, two bigger holes are introduced in the first ring with radius r_b equals to 0.99 μm. As shown in Fig. 8, the radius of the holes in each ring differs from each other and their values are $r_1 = 0.55\,\mu m$, $r_2 = 0.62\,\mu m$, $r_3 = 0.77\,\mu m$ and $r_4 = 0.814\,\mu m$. This structure has been analyzed by the suggested analytical ANN-RBF approach and found to yield a high birefringence value of 0.014 at $\lambda = 1.55\,\mu m$ *by* using circular holes only. Fig. 9 a shows the variation of the birefringence with Λ_x while Λ_y and λ are kept fixed at 2.2 μm and 1.55 μm respectively. As Λ_x increases from 1.65 μm to 2.2 μm, the birefringence decreases from 7.6×10^{-3} to 2.2×10^{-3}. This is due to the fact that the increase in the Λ_x decreases the asymmetry in the structure of the PCF which, in turn, reduces the difference between the effective indices of the two polarized modes. The variation of the birefringence with Λ_y whilst Λ_x and λ are held constant at 2.2 μm and 1.55 μm respectively is demonstrated in Fig. 9b. As Λ_y increases from 1.65 μm to 2.2 μm, the birefringence

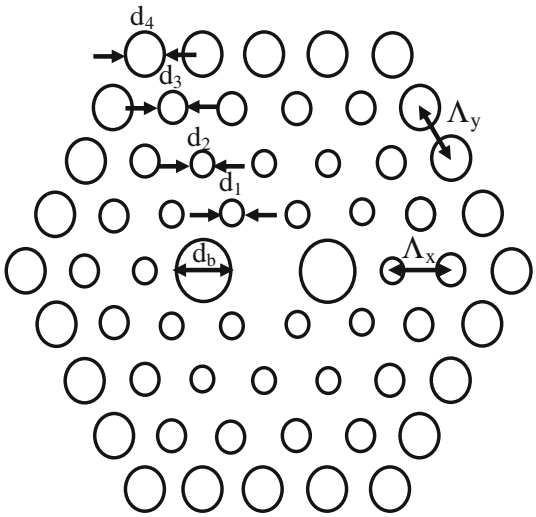

Fig. 8 Cross section of the suggested highly birefringence PCF. The diameters of the holes in each ring are d_1, d_2, d_3 and d_4. However, d_b is the diameter of the two bigger holes in the first ring. Λ_x and Λ_y are the hole pitch in x and y direction respectively

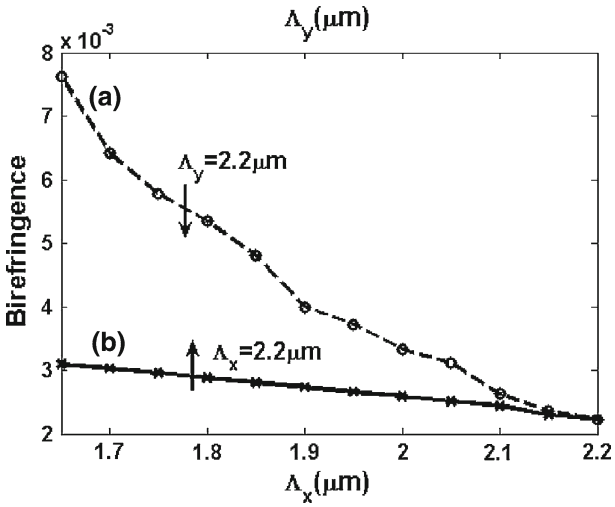

Fig. 9 The variation of the birefringence at $\lambda = 1.55\,\mu m$ with **a** the hole pitch in x-direction Λ_x while the hole pitch in y-direction Λ_y fixed to 2.2 μm **b** Λ_y while Λ_x fixed to 2.2 μm

decreases slightly from 3.1×10^{-3} to 2.2×10^{-3}. It can be concluded from Fig. 9a and b that the squeeze in the x-direction produces higher birefringence than that in the y direction. It should be noted that the birefringence at $\Lambda_y = \Lambda_x = 2.2\,\mu m$ is produced by the two bigger holes in the first ring. Figure 10 a shows that the birefringence decreases with increasing the hole pitch Λ_x from 1.65 μm to 2.2 μm while Λ_y and λ are kept fixed at 1.65 μm and 1.55 μm respectively. The same effect occurs when increasing Λ_y from 1.65 μm to 2.2 μm at constant $\Lambda_x = 1.65\,\mu m$ as shown in Fig. 10b. The variation of the birefringence with the hole pitch $\Lambda_y = \Lambda_x = \Lambda$ is shown in Fig. 10c. It is found that the birefringence decreases by increasing the hole pitch Λ at the operating wavelength $\lambda = 1.55\,\mu m$. It is also evident from Fig. 10a,b and c that the birefringence which occurs due to the squeeze in any direction, is

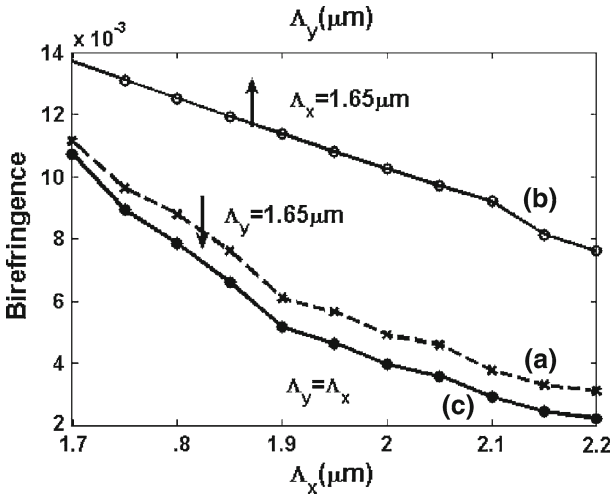

Fig. 10 The variation of the birefringence at $\lambda = 1.55\,\mu m$ with **a** the hole pitch in x-direction Λ_x while Λ_y fixed to $1.65\,\mu m$ **b** Λ_y while Λ_x fixed to $1.65\,\mu m$ **c** hole pitch ($\Lambda_x = \Lambda_y$)

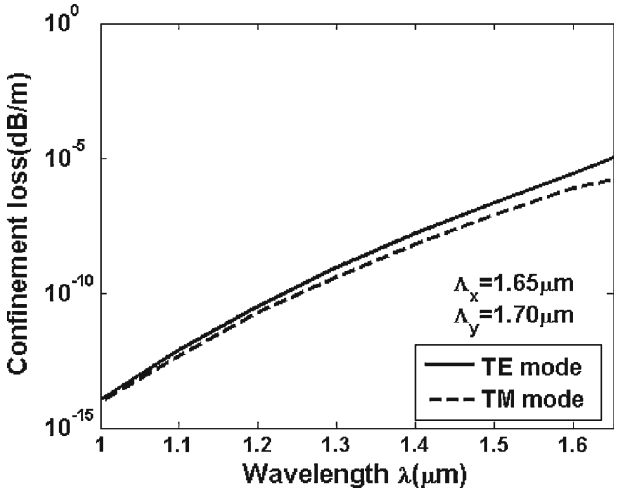

Fig. 11 The variation of the confinement loss of the TE and TM modes with the wavelength while Λ_x and Λ_y fixed to $1.65\,\mu m$ and $1.7\,\mu m$ respectively

greater than the birefringence occurring when Λ_y equals to Λ_x. The proposed structure with $\Lambda_x = 1.65\,\mu m$ and $\Lambda_y = 1.7\,\mu m$ offers high birefringence of 0.014 at $\lambda = 1.55\,\mu m$ with low losses for the two polarized modes by using four rings only. The confinement losses for the TE and TM modes are found to be 5.1×10^{-7}dB/m and 2.26×10^{-7}dB/m respectively at the operating wavelength $1.55\,\mu m$. It is observed that the use of different hole radius in each ring decreases the confinement loss with only four rings. In addition, the losses will be further decreased if additional rings are added. The variation of the confinement losses for the two polarized modes for the proposed PCF with the wavelength is shown in Fig. 11.

The chromatic dispersion which is an important parameter in optical communication systems is considered next. The chromatic dispersion D of a PCF can be calculated from the n_{eff} values versus the wavelength using

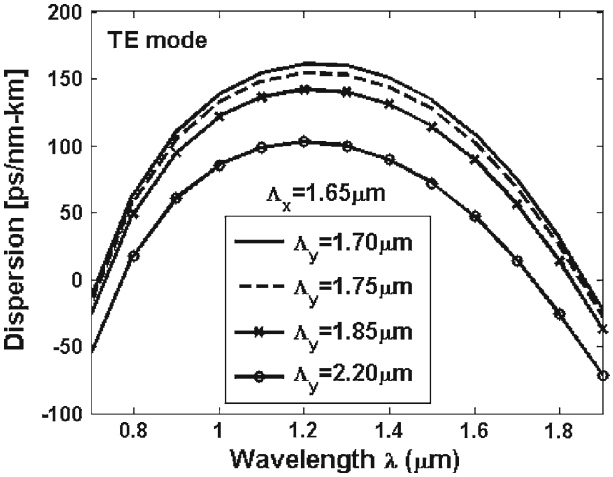

Fig. 12 The variation of the dispersion of the TE mode with the wavelength at different Λ_y values, 1.70 μm, 1.75 μm, 1.85 μm and 2.2 μm, while Λ_x is kept constant at 1.65 μm

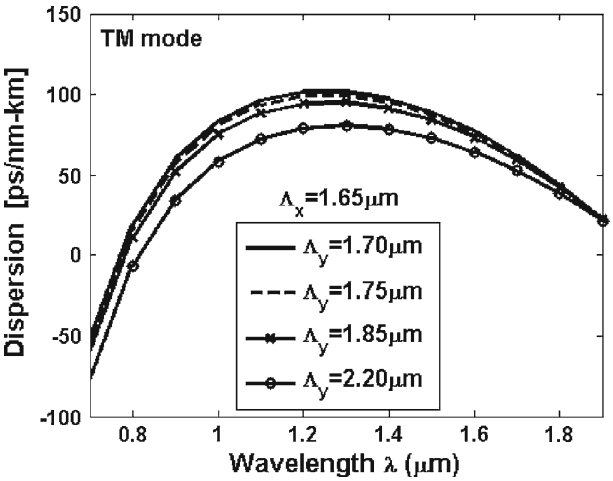

Fig. 13 The variation of the dispersion of the TM mode with the wavelength at different Λ_y values, 1.70 μm, 1.75 μm, 1.85 μm and 2.2 μm, while Λ_x is kept constant at 1.65 μm

$$D = -\frac{\lambda}{c}\frac{d^2 n_{eff}}{d\lambda^2} \tag{11}$$

where c is the velocity of light in the vacuum. The material dispersion given by Sellmeier's formula (Agrawal 1997) is included in the calculation. Figures 12 and 13 show the total dispersion curves of the TE and TM polarized modes, respectively at different Λ_y values while Λ_x is kept constant at 1.65 μm. It is evident from these figures that the shapes of the dispersion curves for both TE and TM modes, show a normal dispersion over a wide range of wavelengths which is believed to be useful for a broadband dispersion compensation. In addition, the normal dispersion for both orthogonal polarizations over a long wavelength ranges decreases with increasing Λ_y. Moreover, the absolute value of the TE dispersion is

larger than that of the TM dispersion. These results agree with those reported previously for elliptical-hole PCF with squeezed lattice (Yue et al. 2007).

4 Conclusion

A new and an accurate artificial ANN-RBF has been suggested for the analysis and design of PCFs. The radial basis function provides a rapid and an accurate learning process. This approach overcomes the meshing problems and time consuming of other numerical modelling methods. A squeezed circular-hole PCF with two big circular air holes adjacent to the core has been proposed which offers a high birefringence of 0.014 at $\lambda = 1.55\,\mu m$ with low losses for the two polarized modes. In addition, a broadband normal dispersion that can be used for broad band dispersion compensation has also been obtained.

References

Agrawal, G.P.: Fiber-Optic Communication Systems, 2nd edn, pp. 41–42. Wiley, New York (1997)

Benabid, F.: Hollow-core photonic bandgap fibre: new light guidance for new science and technology. Philos. Trans. R. Soc. A. **364**, 3439–3462 (2006). doi:10.1098/rsta.2006.1908

Birks, T.A., Knight, J.C., Russell, P.S.J.: Endlessly single-mode photonic crystal fibre. Opt. Lett. **22**, 961–963 (1997). doi:10.1364/OL.22.000961

Broeng, J., Mogilevstev, D., Barkou, S.E., Bjarklev, A.: Photonic crystal fibers: a new class of optical waveguides. Opt. Fiber Technol. **5**, 305–330 (1999). doi:10.1006/ofte.1998.0279

Campbell, S., McPhedran, R.C., Martijnde Sterke, C., Botten, L.C.: Differential multipole method for microstructured optical fibers. J. Opt. Soc. Am. B **21**, 1919–1928 (2004)

Christodoulou, C., Georgiopoulos, M.: Applications of neural networks in electromagnetics. Artech House Publishers, Norwood (2001)

Cohen, L.G., Marcuse, D., Mammel, W.L.: Radiating leak-mode losses in single-mode light guides with depressed-index claddings. IEEE J. Quantum Electron. **18**, 1467–1472 (1982). doi:10.1109/JQE.1982.1071409

Fallahkhair, A.B., Li, K.S., Murphy, T.E.: Vector finite difference modesolver for anisotropic dielectric waveguides. J. Lightwave Technol. **26**, 1423–1431 (2008). doi:10.1109/JLT.2008.923643

Gander, M.J., McBride, R., Jones, J.D.C., Mogilevtsev, D., Birks, T.A., Knight, J.C., Russell, P.S.J.: Experimental measurement of group velocity in photonic crystal fiber. Electron. Lett. **35**, 63–64 (1998). doi:10.1049/el:19990055

Hansen, P., Broeng, J., Libori, E.B., Knudsen, E., Bjarklev, A., Jensen, J.R., Simonsen, H.: Highly birefringent index-guiding photonic crystal fibers. IEEE Photon. Technol. Lett. **13**, 588–590 (2001). doi:10.1109/68.924030

Knight, J.C., Birks, T.A., Cregan, R.F., Russell, P.S.J., de Sandro, J.P.: Large mode area photonic crystal fiber. Electron. Lett. **34**, 1347–1348 (1998). doi:10.1049/el:19980965

Koshiba, M., Saitoh, K.: Polarization-dependent confinement losses in actual holey fibers. IEEE Photon. Technol. Lett. **15**, 691–693 (2003). doi:10.1109/LPT.2003.809923

Lizier, J.T., Town, G.E.: Splice losses in holey optical fibers. IEEE Photon. Technol. Lett. **13**, 794–796 (2001). doi:10.1109/68.935806

Lusse, P., Stuwe, P., Schöule, J., Unger, H.G.: Analysis of vectorial mode fields in optical waveguides by a new finite difference method. J. Lightwave Technol. **12**, 487–494 (1994). doi:10.1109/50.285331

Marcuse Marcuse, D.: Influence of curvature on the losses of doubly clad fibers. Appl. Opt. **21**, 4208–4213 (1982)

Nakazawa, M.: Highly efficient Raman amplification in a polarization preserving optical fiber. Appl. Phys. Lett. **46**, 628–630 (1985). doi:10.1063/1.95508

Obayya, S.S.A., Rahman, B.M.A., Grattan, K.T.V.: Accurate finite element modal solution of photonic crystal fibres. Optoelectronics, IEE Proc. **152**, 241–246 (2005). doi:10.1049/ip-com:20045054

Obayya, S.S.A., Rahman, B.M.A., Grattan, K.T.V., El-Mikati, H.A.: Full vectorial finite-element-based imaginary distance beam propagation solution of complex modes in optical waveguides. J. Lightwave Technol. **20**, 1054–1060 (2001). doi:10.1109/JLT.2002.1018817

Russell, P.S.J.: Photonic crystal fibers. Science **299**, 358–362 (2003). doi:10.1126/science.1079280
Saitoh, K., Koshiba, M.: Empirical relations for simple design of photonic crystal fibers. Opt. Express **13**, 267–274 (2005). doi:10.1364/OPEX.13.000267
Sood, V.K.: HVDC and FACTS Controllers: Applications of Static Converters in Power Systems (Power Electronics and Power Systems), Kluwer Academic, Boston (2004)
Steel, M.J., Osgood, R.M.: Polarization and Dispersive Properties of Elliptical-Hole Photonic Crystal Fibers. J. Lightwave Technol. **19**, 495–503 (2001). doi:10.1109/50.920847
Suzuki, K., Kubota, H., Kawanishi, S., Tanaka, M., Fujita, M.: Optical properties of a low-loss polarization-maintaining photonic crystal fiber. Opt. Express **9**, 676–680 (2001)
Tsai, K.H., Kim, K.S., Morse, T.F.: General solution for stress-induced polarization in optical fibers. J. Lightwave Technol. **9**, 7–17 (1991). doi:10.1109/50.64917
White, T., McPhedran, R., Botten, L., Smith, G., Sterke, C.M.de : Calculations of air-guided modes in photonic crystal fibers using the multipole method. Opt. Express **9**, 721–732 (2001)
Yu, C.P., Chang, H.C.: Applications of the finite difference mode solution method to photonic crystal structures. Opt. Quantum Electron. **36**, 145–163 (2004). doi:10.1023/B:OQEL.0000015636.20125.7e
Yue, Y., Kai, G.Y., Wang, Z., Sun, T.T., Jin, L., Lu, Y.F., Zhang, C.S., Liu, J.G., Li, Y., Liu, Y.G., Yuan, S.Z.: Highly birefringent elliptical-hole photonic crystal fiber with two big circular air holes adjacent to the core. IEEE Photon. Technol. Lett. **18**, 2638–2640 (2006). doi:10.1109/LPT.2006.887330
Yue, Y., Kai, G., Wang, Z., Sun, T., Jin, L., Lu, Y., Zhang, C., Liu, J., Li, Y., Liu, Y., Yuan, S., Dong, X.: Highly birefringent elliptical-hole photonic crystal fiber with squeezed hexagonal lattice. Opt. Lett. **32**, 469–471 (2007). doi:10.1364/OL.32.000469